Geosystems and Geoenvironment 2 (2023) 100211

Contents lists available at ScienceDirect

Geosystems and Geoenvironment

journal homepage: www.elsevier.com/locate/geogeo

Fault dip vs shear stress gradient

Davide Zaccagnino [a], Carlo Doglioni [a,b,*]

[a] Department of Earth Sciences, Sapienza University, P.le Aldo Moro 5, Rome 00185, Italy
[b] National Institute of Geophysics and Volcanology, Via di Vigna Murata 605, Rome 00143, Italy

ARTICLE INFO

Article history:
Received 31 May 2023
Revised 14 June 2023
Accepted 14 June 2023

Handling Editor: Sanzhong Li

Keywords:
Fault dip
Tectonic settings
Shear stress gradients

ABSTRACT

In the brittle regime, faults tend to be oriented along an angle of about 30° relative to the principal stress direction. This empirical Andersonian observation is usually explained by the orientation of the stress tensor and the slope of the yield envelope defined by the Mohr-Coulomb criterion, often called critical-stress theory, assuming frictional properties of the crustal rocks ($\mu \approx 0.6–0.8$). However, why the slope has a given value? We suggest that the slope dip is constrained by the occurrence of the largest shear stress gradient along that inclination. High homogeneous shear stress, i.e., without gradients, may generate aseismic creep as for example in flat decollements, both along thrusts and low angle normal faults, whereas along ramps larger shear stress gradients determine higher energy accumulation and stick-slip behaviour with larger sudden seismic energy release. Further variability of the angle is due to variations of the internal friction and of the Poisson ratio, being related to different lithologies, anisotropies and pre-existing fractures and faults. Misaligned faults are justified to occur due to the local weaknesses in the crustal volume; however, having lower stress gradients along dip than the optimally-oriented ones, they have higher probability of being associated with lower seismogenic potential or even aseismic behavior.

1. Introduction

In his seminal papers, Anderson (1951, 1905) described the dip relation of faulting depending on the tectonic style. He focused on the angle of dip, suggesting that 90° be the optimal for strike-slip faults, around 60° for normal faults, and 30° along thrusts. This observation was and is still today largely coherent with the field and seismic data in the brittle upper crustal deformation, and the orientation of the maximum stress tensor (σ_1), that is, on average, at an angle of $\sim 30°$ with respect to the fault plane in the three main tectonic settings. Internal static friction, lithological heterogeneity, inherited anisotropy, and fluid pressure play a fundamental role in controlling the variability of fault dip that may significantly deviate from the theoretical angle (e.g., Fossen, 2016). Some models challenge the Anderson model, being supported by mechanical theory and by experiments. For example, a unique fault geometry is suggested to develop under the case of 3D strain field (Reches, 1983; Reches and Dieterich, 1983). In this case, orthorhombic system is predicted to develop on pre-existed frictional surfaces with slip orientations that substitute the minimum stress difference and the minimum frictional dissipation in a given strain field. However, any model with spatially constant boundary conditions and initial conditions (i.e., no pre-stress, same material properties everywhere in a flat plate) and a yield envelope with a constant slope will always produce faults with a constant dip angle (Twiss and Moores, 1992). This research aims to highlight the importance of pressure gradients in determining fault dip, i.e., the slope of the yield envelope defined by the Mohr-Coulomb criterion, or tangent modulus in continuum-mechanics, and the most seismogenic segments of tectonic planes. A gradient describes the variation in space and time of any physical parameter (e.g., Aifantis, 2020). The strongest the gradient of the potential, the higher the force acting on the system. Therefore, the highest stress gradients in the crustal volume correspond to the largest concentration of potential energy (Zaccagnino and Doglioni, 2022a). We focus on the normal and shear stress gradients along different fault dips as a function of the tectonic setting and the related three principal stresses, being the vertical one coincident with the lithostatic load. Tectonic settings are featured by several differences regarding structural properties of the fault

* Corresponding author.
E-mail address: carlo.doglioni@uniroma1.it (C. Doglioni).

https://doi.org/10.1016/j.geogeo.2023.100211

zone, fluid circulation (Sibson, 1994), statistical patterns of seismicity (Zaccagnino et al., 2022), components of moment tensors of earthquakes (Zaccagnino and Doglioni, 2022b) and stress accommodation. Once again, these occurrences show contrasting patterns as a function of the tectonic setting (Doglioni et al., 2014). Nevertheless, the asymmetry described above is a matter of fact and various physical mechanisms have been proposed for explaining it. Starting from the criterion for frictional failure described by the Amonton's law, taking into account of fluid pressure P_f, i.e., for sliding to occur, shear stress τ must overcome friction μ

$$\tau \geq \mu(\sigma_n - P_f) \tag{1}$$

where σ_n is the normal stress, under the hypothesis of aggregate materials with negligible cohesion (faulting already developed), Sibson (1974) derived the vertical profiles for differential stress in the three tectonic regimes given by

$$\sigma_1 - \sigma_3 = \beta\rho g z(1-\lambda) \tag{2}$$

where β is about 0.75, 1, and 3 respectively in normal, strike-slip and reverse faulting, being a function of the friction coefficient μ via the optimal ratio

$$\left(\frac{\sigma_1}{\sigma_3}\right)_{min} = \left(\sqrt{1+\mu^2} - \mu\right)^{-2}. \tag{3}$$

λ is a parameter representing the ratio of pore fluid pressure over vertical (overburden) stress; its value can range in between 0 and 1, for modeling purposes $\lambda = 0.4$ is usually assumed Ranalli (1995). Therefore, the result above is achieved assuming that slip completely occur on a single planar, pre-existing fault surrounded by elastic cohesive rocks; hence, that the frictional properties of the interface completely control the entire "seismic cycle". In the same framework, the optimal angle of dip for faulting is also obtained, being respectively 55°–60° and 25°–30° for extensional and contractional tectonic settings. The optimal angle between the direction of principal stress and slip direction is given by

$$\vartheta = \frac{1}{2}\arctan\left(\frac{1}{\mu}\right) \tag{4}$$

where it is usually assumed $\mu = 0.6–0.8$ (Byerlee, 1978), so that $\vartheta \sim 25-30°$. However, geodetic inversion of strain in faulting regions suggest much lower average friction coefficients, usually ≤ 0.3 (Bird and Kong, 1994) and sometimes even more reduced ones, with $\mu \sim 0.01–0.1$ (e.g., Dal Zilio et al., 2019). Similar outputs are provided by laboratory and geological observations (Collettini et al., 2019). Those static friction values are often associated with weak lithology and generally occurring along low-angle fault planes. The presence of weak fault gouges or fluid overpressure is also utilized to justify observed heat flux during fault slip (dynamic friction), which would otherwise be incompatible with faulting (Hickman, 1991). In the latter case, would be quite difficult to relate friction (friction laws turn out to be dependent on model and spatial-temporal scale of observation) to the angle of dip according to Eq. (4). In this regard, should be noticed that, at very low friction coefficients ($\mu \to 0$), both thrusts and normal faults are predicted to have a dip of $\approx 45°$. This straightforward consequence implies that low-friction faults, regardless of their tectonic setting, are expected to have the same intermediate angle of dip, which is in contrast with the evidence of low-angle normal faulting, usually explained in light of anomalously weak frictional interfaces (e.g., Axen, 1992; Collettini, 2011) and gently vs steeply dipping thrusts along subduction zones (Tan et al., 2012). By the way, low-magnitude seismic activity of low-angle normal faults has been suggested to be due to stress rotation with depth due to tensile components and vertical viscosity gradients (Melosh, 1990; Westaway, 1999) or simply due to the minor vertical (gravitational) component of the coseismic slip (Doglioni et al., 2015). However, the first hypothesis is unsubstantial, since tensile stress components disappear below about one kilometer of depth (Twiss and Moores, 1992), while the second is not exhaustive since active faults with low dip are also observed at shallow depth. In the same context, the paradox of large thrusts dipping at very small angles ($\leq 10°$) requires an almost negligible shear friction with respect to what should be expected using the Byerlee's law (Anooshehpoor and Brune, 1994), also resulting incompatible with the Andersonian model of faulting. Ranalli and Yin (1990) expanded the Sibson theory, deriving equations for the critical stress difference on thrust, normal and strike-slip faults with finite cohesive strength, both in homogeneous, isotropic rock, and along pre-existing strength anisotropies with different cohesion and coefficient of friction. Yin and Ranalli (1992) further describe variations of the fault dip in anisotropic rocks under non-Andersonian stress. Even more advanced evolution in the matter is in Healy et al. (2015) describing polymodal faulting of shear failure. In this research, we study the shear stress gradient along faults in the three principal tectonic settings, discuss the energy source of the faults activation and provide an alternative explanation for the most frequent fault dip being controlled by the concentration of the largest pressure gradient in the upper crustal volume.

2. Model

2.1. Preliminary observations and theory

The brittle lithosphere undergoes several stress sources: the lithostatic stress, $\sigma_v = \rho g z$, where $\rho \sim 2.65$ g/cm^3 and z represents the depth, is produced by the weight of the layers of rocks above the reference level, the tectonics stress, σ_t, due to the lateral compressive action of contiguous plates and thermal stress $\sigma_H = Y\alpha_T(\Delta T)/(1-\nu)$, where Y is the Young's modulus and $0 \leq \nu \leq 0.5$ represents the Poisson's modulus, takes into account of thermal gradients, ΔT, inside the crust. In the present work, we neglect the first term, assuming thermal gradients be negligible with respect to other stress sources. Because of the elastic properties of rocks, the vertical lithostatic stress is transmitted to the horizontal direction as $\sigma_h = \nu\rho g z/(1-\nu)$. However, since upper layers show dynamical behaviors incompatible with pure lithostatic loading (Scholz, 2019), rocks exhibit porosity so that the vertical component of stress is redistributed over a contact area determined by the interactions of heterogeneously-shaped grains of solid material embedded in a weaker matrix filled with circulating fluids. As a consequence, the Janssen's model (Sperl, 2006) for granular materials gives

$$\sigma_v(z) = \rho g L_c\left(1 - e^{-z/L_c}\right) \tag{5}$$

where is a characteristic length controlling the scale of pressure saturation. The formula above can be expanded in Taylor series up to the second order in the neighborhood of depth $z = 0$, since we are interested in the state of stress in the brittle lithosphere up to a few kilometers below the surface, being the information about the effective state of stress inaccurate beyond such depths (Brudy et al., 1997). So, we get

$$\sigma_v(z) = \rho g L_c\left(1 - e^{-z/L_c}\right) \simeq \rho g z\left(1 - \frac{z}{2L_c}\right) \tag{6}$$

which is in good agreement with observations (e.g., Shebalin and Narteau, 2017). At last, we can write Eq. (6) in a more familiar way assuming pore pressure be independent from depth for modeling purposes (even though unreliable); therefore, we reach the well-know formula $\sigma_v = \rho g z(1-\lambda)$. Then, the vertical stress is reduced

by the action of pore pressure by a factor λ. For modeling purposes, in the next paragraph we assume that two sources of stress act on the system: the vertical lithostatic stress and the horizontal compressive tectonic stress; furthermore, the mechanical rigidity of the system allows transmission of stress components in the orthogonal direction. For modeling normal-faulting regions, it is assumed $\sigma_1 = \sigma_v$, conversely, $\sigma_3 = \sigma_v$ in compressive settings, while $\sigma_2 = \sigma_v$ for transcurrent plate boundaries. The major principal axis corresponding to the direction of σ_1 is the horizontal one in compressive regions producing angles of dip lower than 45°, while it is the vertical one in extensional tectonic settings, where faults are steeper ($\geq 45°$). In the first case, the driver of local dynamics is the tectonic stress, conversely, gravity controls faulting in the second one. This simple model corresponds the so-called Rankine's criterion (Lagioia and Panteghini, 2016) applied for the modeling of granular matter. It also assumes that the tectonic stress is constant as a function of depth, which is not a reliable request. Nevertheless, it provides a simple explanation for different angles of dip taking into account of both frictional and granular properties of the matter; the dip is expected to be $(45 \pm \delta/2)°$ respectively in the extensional and compressive case. δ represents the angle of friction accounting for pure frictional, geometrical and dilatant contributions to resistance to sliding. Notice that no elastic tensile stress is required for normal-faulting dynamics; moreover, no elastic strain is accumulated during the interseismic and preseismic phase, while dilatancy takes place in broadly fractured zones which become progressively filled with fluids, above all inside the volumes undergoing larger preseismic deformations (Jackson and White, 1989). Liquids are ejected from the porous medium once the fractures tend to close as a consequence of slip, which is compatible with observed fluid circulation in extensional tectonic settings (Doglioni et al., 2014).

In this model, the whole energy budget for normal faulting is provided by gravity coherently with several works about extensional tectonics (Dewey, 1988; Doglioni et al., 2015; Fazlikhani et al., 2017; Kapp et al., 2008; Leech, 2001; Livaccari, 1991; Wernicke and Axen, 1988). By a seismological viewpoint, during the preseismic phase, rock volumes located along and beside the weaker interface, i.e., the fault, undergo localized strain which tends to dislodge them from their previous state of equilibrium, producing an elastic, rotating stress field opposing the horizontal withdrawal of mass from the fault zone due to dilatancy and thus to the unloading of the foot-wall. Experiments in the lab support the actual occurrence of this process (Cartwright-Taylor et al., 2022) as well as geophysical analyses (Faulkner et al., 2006); moreover, geological fabric associated with normal faulting, e.g., S-C structures, prove the action of rotational strain (e.g., Morley et al., 2004; Schueller et al., 2013; Wang et al., 2014). This phenomenon guarantees the action of perpendicular force dipoles producing a pattern of tensile and compressive stress over the fault plane of sliding, thus, still a double-couple mechanism for normal-faulting earthquakes (Thompson and Parsons, 2017). In the next paragraph, we apply this framework for deriving the optimal angle of dip for faulting with an alternative approach to classical friction.

2.2. Optimal dip angles of faults

We can use the considerations discussed above for deriving the optimal angle of dip of earthquakes in different tectonic settings in the brittle crust. In the case of extensional tectonics, at seismogenic depths, i.e., few kilometers below the surface, no tensile stress acts (Doglioni et al., 2015; Twiss and Moores, 1992), but the gravitational load is spread in the horizontal direction via the elastic Poisson's parameter ν, i.e., the confining pressure.

$$\begin{cases} \sigma_v = (1-\lambda)\rho g z \\ \sigma_h = (1-\lambda)\dfrac{\nu}{1-\nu}\rho g z \end{cases} \tag{7}$$

We can evaluate the normal component of stress σ_n acting on an ideal planar fault with dip angle α and estimate its mechanical work per surface unit

$$w = \int_0^s \sigma_n \, dl \tag{8}$$

along a displacement with length $l = s$ in the slip direction. A straightforward integration gives $w = s\left[(1-\lambda)\rho g \sin(\alpha)\cos(\alpha) + \frac{\nu}{1-\nu}(1-\lambda)\rho g \sin^2(\alpha)\right]$; setting $s = 1$ for the sake of simplicity, we can find the optimal angle by maximizing w as a function of the dip angle. So, we impose the condition $\frac{\partial w}{\partial \alpha} = 0$. We get

$$\alpha_o = 90^\circ + \frac{1}{2}\arctan\left(\frac{\nu - 1}{\nu}\right). \tag{9}$$

Using 0.25, we obtain $\alpha_o \approx 54°$, which is in good agreement with field observations and resolved fault plane dip angles retrieved by solutions of focal mechanisms of moderate and large earthquakes. Notice that the porosity λ does not affect the angle of dip, therefore, for our purposes, it can be set at an arbitrary value. Fig. 1 shows the normal stress gradient along normal-fault slip as a function of the dip angle according to our model.

The probability that a large earthquake takes place along a fault featured by a given dip angle α instead of its optimal value α_o decreases exponentially as a function of the angular misalignment $|\alpha - \alpha_o|$. Since the profile in Fig. 1a is not narrowly picked around its maximum, normal-faulting earthquakes routinely occur within a wide range of dip angles, namely in between 40° and 70°. However, values of dip up to 90° or down to $15 - 20°$ are not impossible, although less probable. We can proceed analogously for finding the optimal angle of dip for thrusts. In this case, we must take into account not only of the lithostatic loading but also of the horizontal compressive stress due to the gradient of viscosity between contiguous plates. It is assumed to be linearly dependent on depth $\sim \kappa z$ where $\kappa \approx 75$ MPa/km, but it can be extremely variable depending on several factors such as the presence of fluids. κ represents the vertical tectonic stress gradient, i.e., how the horizontal tectonic stress increases as a function of depth.

$$\begin{cases} \sigma_v = \rho g z(1-\lambda) - \dfrac{\nu}{1-\nu}(1-\lambda)\kappa z \\ \sigma_h = \dfrac{\nu}{1-\nu}(1-\lambda)\rho g z + \kappa(1-\lambda)z \end{cases} \tag{10}$$

We can now calculate the amount of work done by the normal component of stress acting on a thrust with dip angle α and along a displacement of length s in the slip direction (upward in this case). Imposing null derivative with respect to α for the work density w along the fault and taking its minimum value, we get

$$\alpha_o = -\frac{1}{2}\arctan\left(\frac{\rho g + \frac{\nu}{1-\nu}\kappa}{\frac{\nu}{1-\nu}\rho g + \kappa}\right). \tag{11}$$

Using 0.25, we obtain $|\alpha_o| \approx 16°$, which is coherent with geological observations (thrust faulting is usually featured by angles of dip ranging in between $5°-30°$) and resolved fault plane dip angles inferred from focal mechanisms of large earthquakes. Compare with Fig. 2.

It is worth to stress that the value of the optimal angle for thrusts is strongly dependent on the assumptions about the vertical gradient of the compressive tectonic stress. In particular, the optimal angle increases as the vertical gradient of stress decreases.

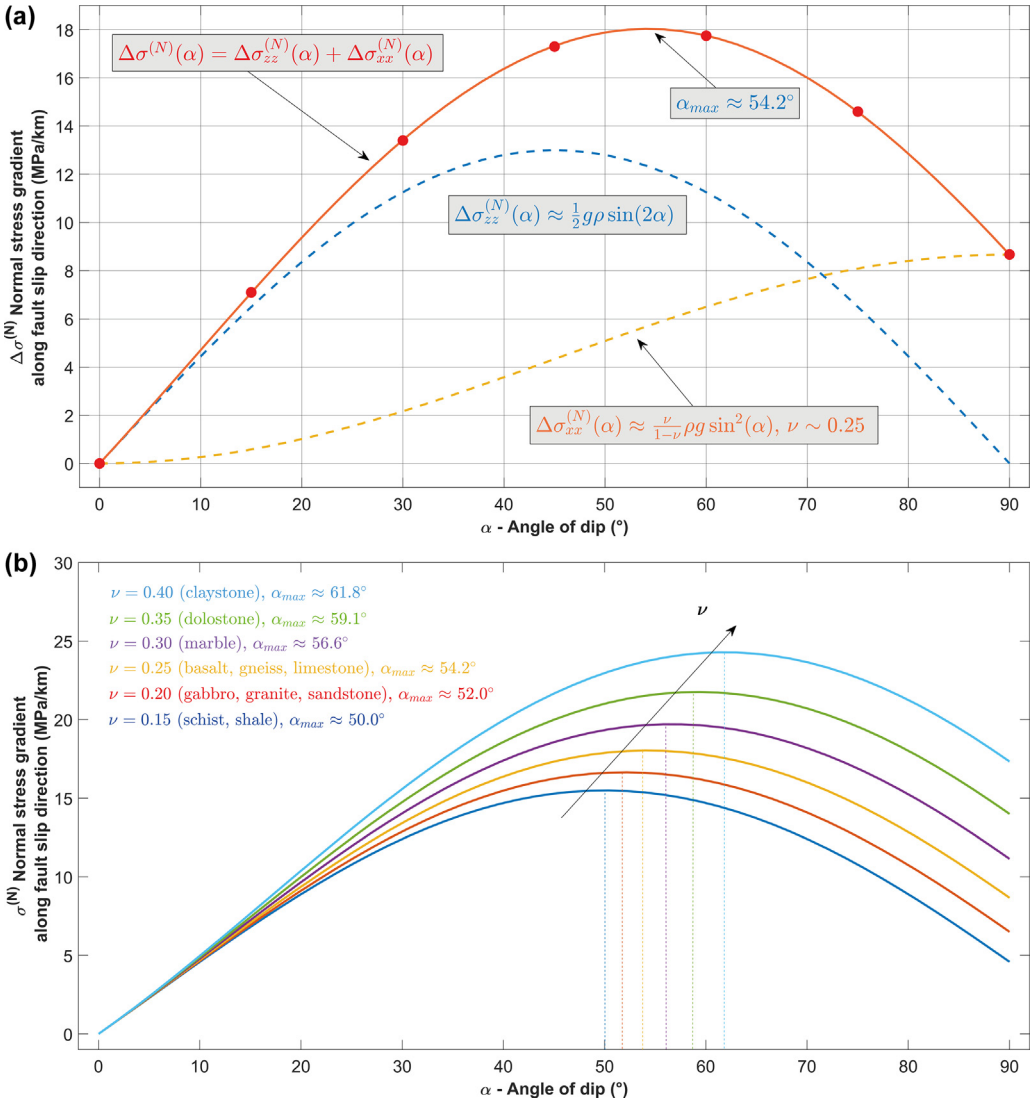

Fig. 1. Normal stress gradient along normal-fault slip. Plot realized using $\lambda = 0$. (a) The gradient as a function of the angle of dip and its horizontal and vertical components; (b) the gradient depends on the Poisson's ratio ν. The optimal angle of dip is about 54°.

In the limit case of null gradient, meaning a perfectly locally uniform tectonic stress with depth, the optimal angle $\alpha_o \to 36°$, which is the complementary angle of 54°, which is reasonable, being this special situation the symmetric one with respect to normal-faulting, with axes rotated by 90° ($\sigma_1^{(normal)} \equiv \sigma_1^{(thrust)}$). Compare with Fig. 3. Being the profile of the normal stress gradient not steep around its extreme value, thrust-faulting earthquakes can occur along fault with differently dips in between 0° and 40° or even larger.

Transcurrent events cannot be modeled using a simple two-dimensional stress profiles, so we need to add a third direction, being that of the strike of the fault as follows

$$\begin{cases} \sigma_v = \rho g z(1-\lambda) \\ \sigma_h^{(n)} = \dfrac{\nu}{1-\nu}(1-\lambda)\rho g z - \dfrac{\nu}{1-\nu}\kappa(1-\lambda)z \\ \sigma_h^{(s)} = \dfrac{\nu}{1-\nu}(1-\lambda)\rho g z + \kappa(1-\lambda)z \end{cases} \tag{12}$$

However, only the second component can directly affect the angle of dip of pure strike-slip-faulting earthquakes since the third acts parallel to the fault plane by definition and vertical offsets are not considered here. Hence, the optimal angle can be obtained, by using the same steps followed above for the other tectonic settings, considering only of the second contribution. The final results is $\alpha_o = 90°$.

3. Analysis

Assessing the real distribution of dip angles α is a delicate issue because of the limited amount and quality of available information; moreover, data are often representative of few selected, well-studied tectonic regions. Here, we analyze 273 large worldwide earthquakes in different tectonic settings (GCMT catalog, 1990-2021, $M_W \geq 7.0$, depth ≤ 50 km, intra-slab and volcanic events removed). For each earthquake, given its focal mechanism, the most appropriate angle of dip is attributed combining source mechanism (USGS catalog), geological and geophysical information with man-made checking. We compare the statistical results of our analysis with the predictions of our model. To do so, we must convert the difference of normal stress gradients (integrated along a normalized distance according to the setting $s = 1$) with respect to their optimal values α_o into a probability of misalignment $\alpha - \alpha_o$ of the dip angle α. We use a classical Gibbs approach assuming an exponential reduction of frequency as a function of the angular mis-

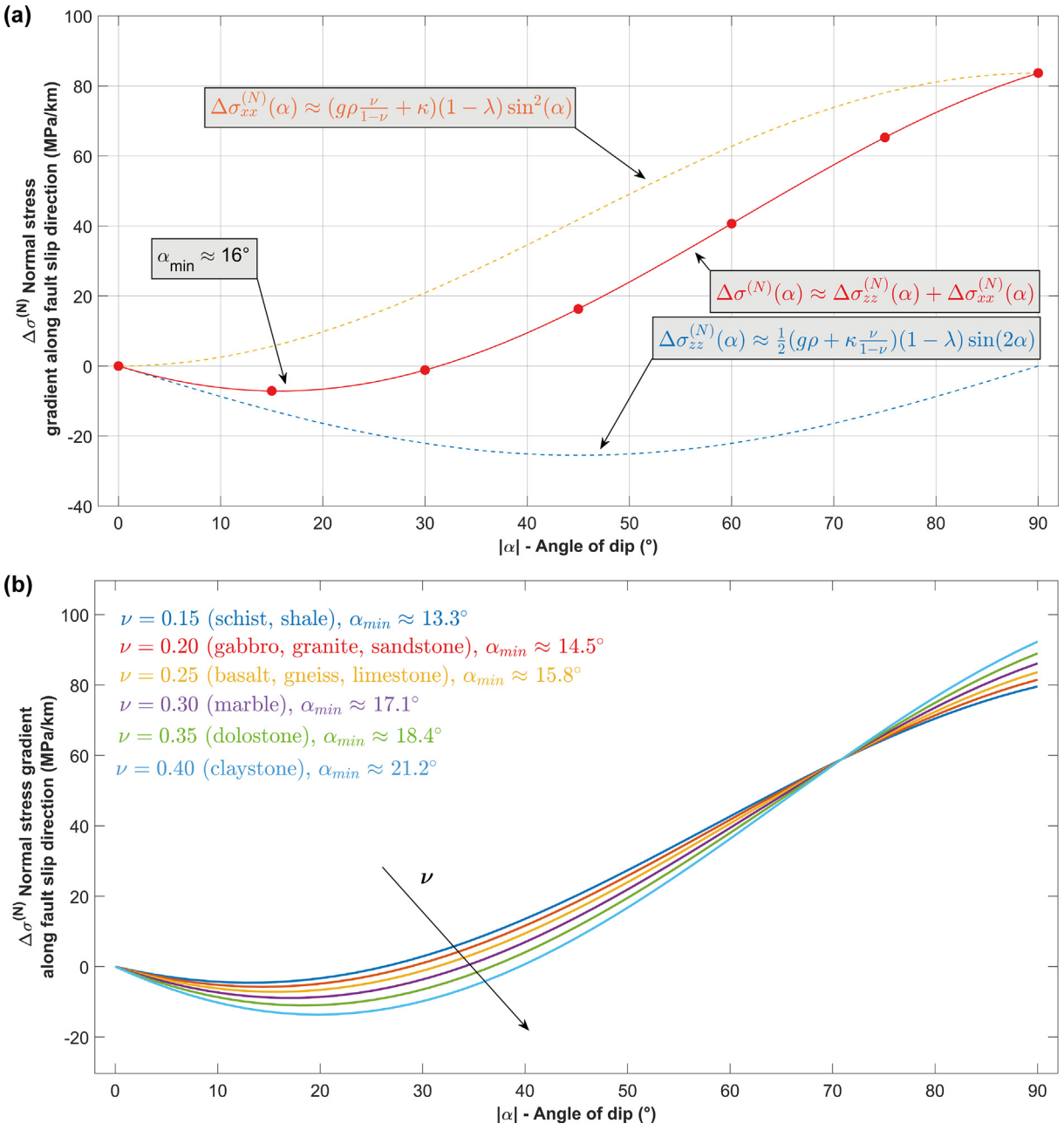

Fig. 2. Normal stress gradient along reverse-fault slip. Plot realized using $\lambda = 0$. The optimal angle of dip is around 16°. (a) The gradient as a function of the angle of dip and its horizontal and vertical components ($\nu = 0.25$, $\kappa = 75$ MPa/km); (b) the gradient depends on the Poisson's ratio ν.

alignment, according to the formula

$$p(\alpha) = \frac{e^{-\beta|\Delta\sigma_N(\alpha) - \Delta\sigma_N(\alpha_o)|}}{\int_0^{\pi/2} e^{-\beta|\Delta\sigma_N(\alpha) - \Delta\sigma_N(\alpha_o)|} d\alpha}, \tag{13}$$

where β is a free parameter of fit.

4. Results and discussion

The distribution of dip angles of faults is a thorny topic: even though it is well known that thrusts have lower dips than rifts, analyses are usually based on few cherry-picked faults and selected solutions of focal mechanisms of large earthquakes; therefore, even though reasonable, several results lack statistical significance being representative of regional tectonic structures and not of a whole faulting type. Moreover, uncertainties are large. In order to compare our theoretical results with observations, we need large number of seismic events all over the Earth. We selected about three hundred large ($M_w \geq 7$) crustal non-volcanic earthquakes occurred from 1990 to 2021 and listed in the USGS and GCMT catalogs; for each event, we inferred the fault plane using the best solution of focal mechanism, geological (mapped faults, geological setting) and geophysical data (e.g., spatial distribution of aftershocks, finite fault slip inversions). Thus, we get a well-supplied database representing faulting associated with major worldwide seismicity. Our results, displayed in Fig. 4, show a substantial agreement between our model and observations, as already proposed by Anderson (1951). However, our interpretation relates these dips to the distribution of the largest shear stress gradient.

We also consider the distribution of magnitudes as a function of dip angles for the same set of large worldwide earthquakes in different tectonic settings (Fig. 5). Even though the dataset is limited, it is representative of the large magnitude events occurred dur-

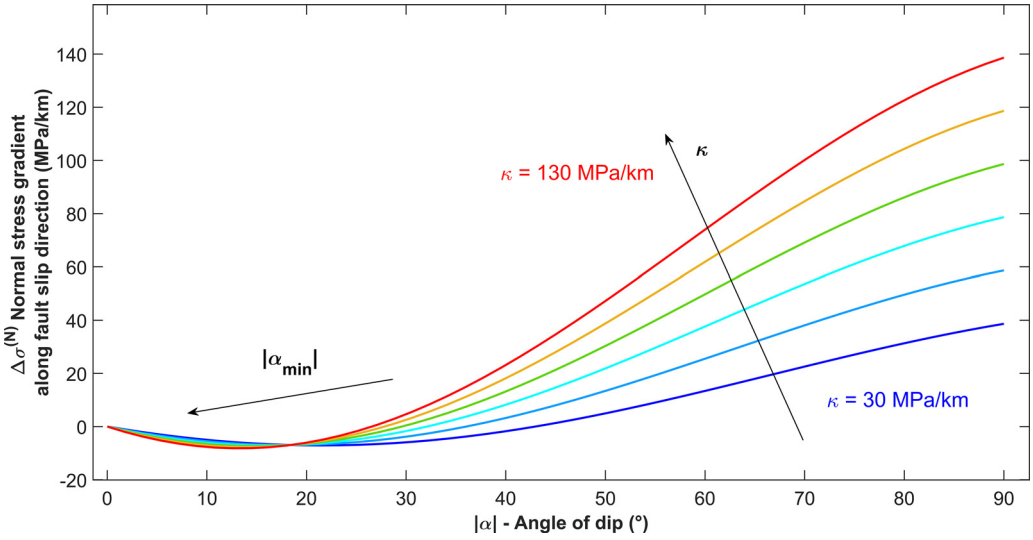

Fig. 3. Normal stress gradient along reverse-fault slip as a function of the angle of dip at different values of the vertical gradient of σ_1, κ ($\nu = 0.25$).

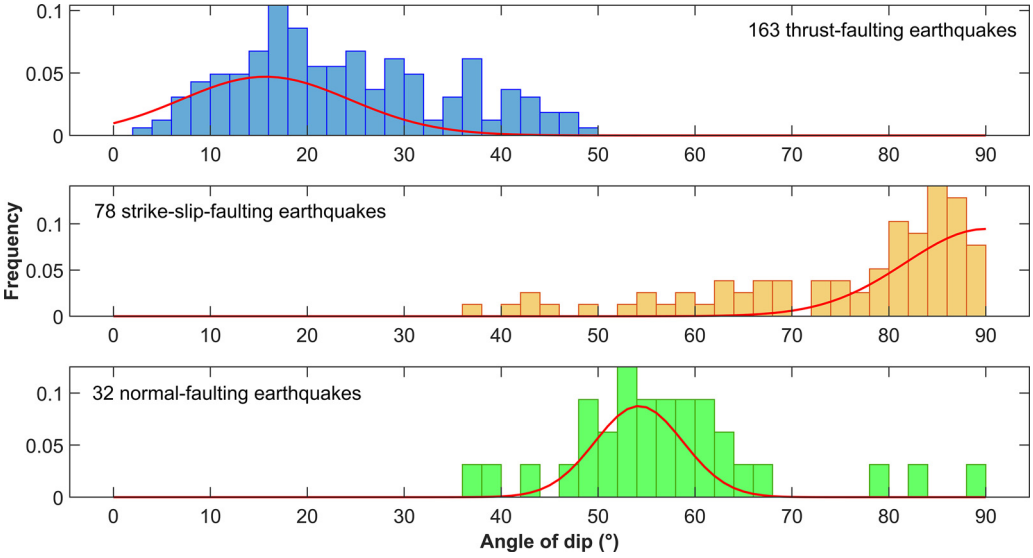

Fig. 4. Distribution of dip angles for large worldwide earthquakes in different tectonic settings (GCMT catalog, 1990-2021, $M_w \geq 7.0$, depth ≤ 50 km, intra-slab and volcanic events removed). For each earthquake, given the focal mechanism, the most appropriate angle of dip is attributed combining source mechanism (USGS catalog) and geological information. The red lines represent the best fitting curves for the probability density function $p(\alpha)$ associated with the model introduced in the present article according to an exponential weight $p(\alpha) \propto \exp(-\beta|\Delta\sigma_N(\alpha) - \Delta\sigma_N(\alpha_o)|)$, β is left as the fit free parameter. Our model correctly reproduces the observed distributions.

ing the last three decades. The largest thrust-faulting events take place along low-dip-angle faults, with a clear decreasing trend; on the contrary, transcurrent faults nucleate the most energetic earthquakes dipping almost perpendicularly to the horizontal reference. No clear trend is found for normal-faulting earthquakes, likely because of insufficient statistics; however, it is well known that low-angle normal fault usually are featured by limited seismogenic potential (Wernicke and Axen, 1988), which is coherent with the source of energy budget in extensional tectonic regimes, i.e., mainly gravitational (Doglioni et al., 2015). In the latter case, further analysis with statistical significance is required, even though evidence has already been provided that only few normal-faulting events occur along faults with low angles of dip and with small to moderate magnitudes (Collettini, 2011).

The results above suggest that some differences between faulting in tectonic settings such as the angle of dip can be explained in the light of the spatial stress gradients acting in the brittle crust, without invoking additional frictional properties of faults and fluid circulation, even though they can be still considered for better understanding the mechanics of peculiar conditions. In particular, it is shown that they not only play a role in selecting the most probable angle of dip, but also modulate the magnitude of (at least) large events, being the largest thrust-faulting events expected along gently-dipping faults, while, conversely, major normal- and strike-slip-faulting events respectively mostly happen along high-angle and vertical fractures. A visual explanation in terms of spatial shear gradients along dip is given in Fig. 6 and Fig. 7.

At last, stress gradients can also be useful to explain other poorly investigated evidence. For instance, it is well known that moderate to large magnitude thrust-faulting earthquakes mostly occur along ramps, where the spatial shear gradient is maximum, while only aseismic creep or small to moderate magnitude seismicity takes place along the flat decollement, which is indeed featured by an extremely limited spatial shear stress gradient (Fig. 8).

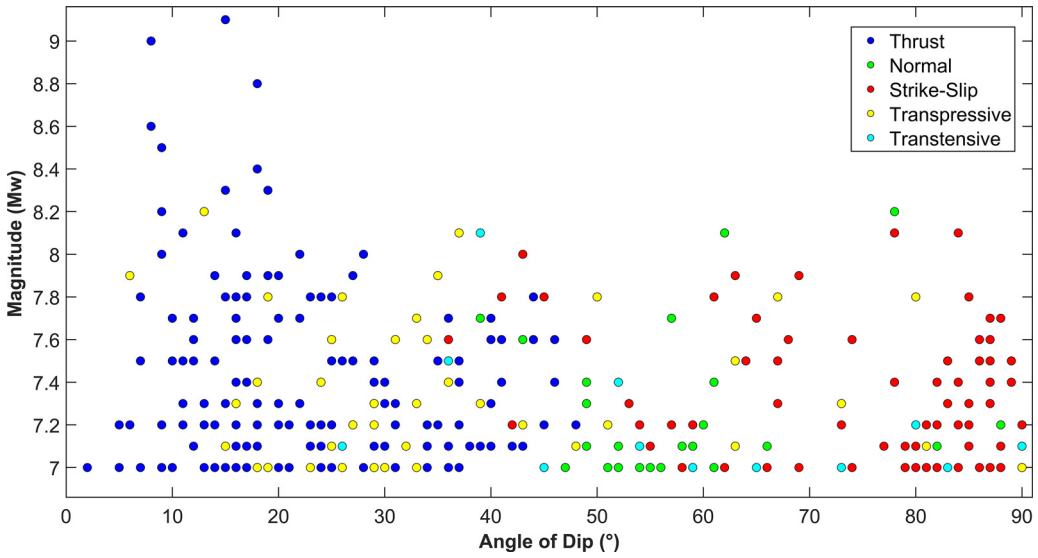

Fig. 5. Distribution of magnitudes as a function of the dip angle for large worldwide earthquakes in different tectonic settings (GCMT catalog, 1990-2021, $M_w \geq 7.0$, depth ≤ 50 km, intra-slab and volcanic events removed). The largest thrust-faulting events take place along low-dip-angle faults; on the contrary, transcurrent faults nucleate the most energetic earthquakes dipping almost perpendicularly to the horizontal reference.

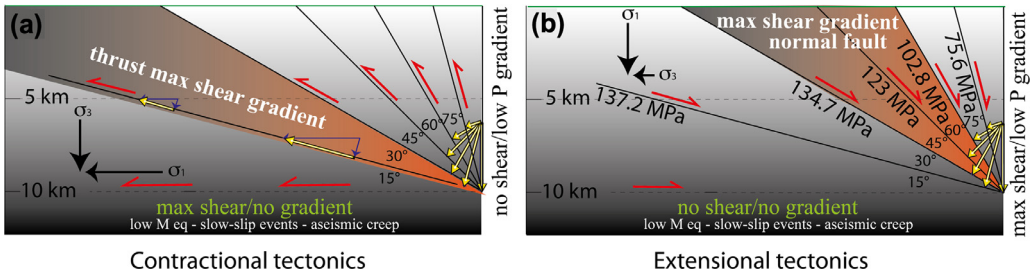

Fig. 6. Assuming a constant friction, the shear stress gradient controls the fault dip. Notice how the shear stress gradient is maximum at the typical thrust (a) and normal fault (b) dips. Along a thrust flat the shear stress is maximum, but the gradient is null in case of homogeneous friction parameters. This allows hanging wall creeping or slow-slip events. Numbers in panel (b) indicate the normal stress variation at 5 km depth acting on the fault plane as a function of the normal fault dip due to the lithostatic load.

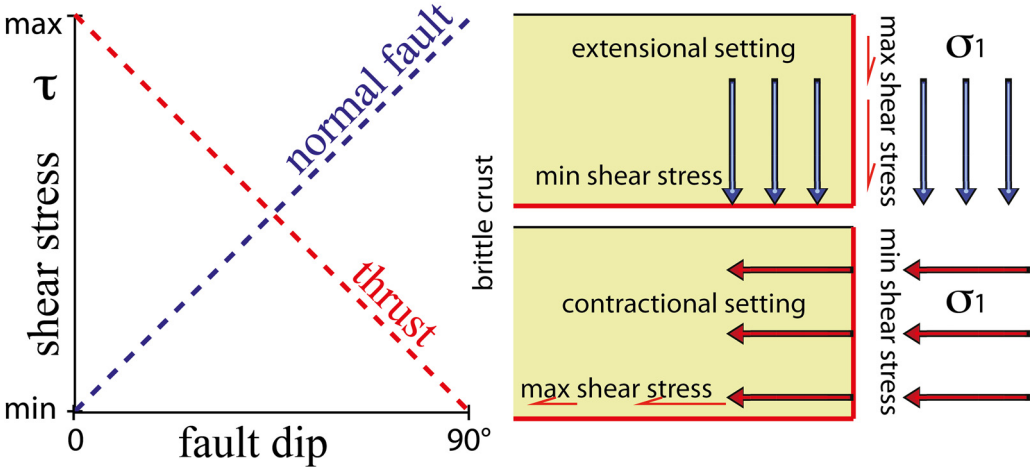

Fig. 7. In the extensional tectonic setting, the shear stress is maximum at 90° because the maximum stress tensor is vertical, i.e., the lithostatic load, but the gradient is low, whereas at 0° there is no shear stress. In the contractional setting, the shear stress is the highest at 0°, whereas at 90° there is no shear stress. The maximum shear stress gradient occurs between about 45°–60° for extensional tectonic settings and at 10°–30° in contractional settings.

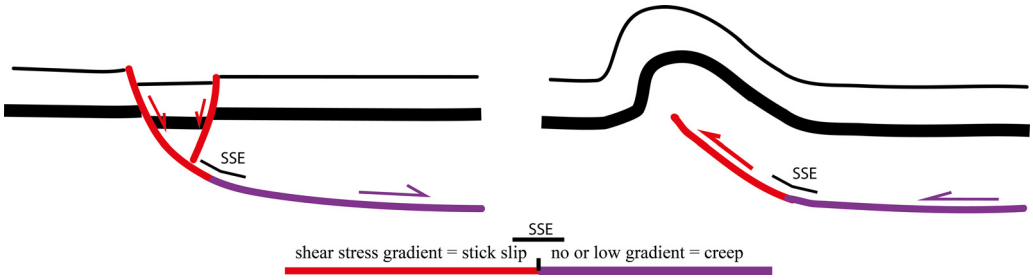

Fig. 8. Due to the presence of low-friction layers, low-angle/flat decollement in extensional and contractional settings allow fault creep or slow-slip events (SSE), without stick-slip motion, whereas earthquake nucleation occurs more frequently along ramps where there is a shear stress gradient, i.e., larger energy accumulation and stick-slip behaviour.

5. Conclusions

This research presents a new model suggesting that the angles of tectonic faults are determined by the value of the shear stress gradient acting in the brittle crustal volume. This idea complements previous knowledge on friction and faulting. Different combinations of stress sources produce the wide range of faulting styles routinely observed in the brittle lithosphere. Geological and seismological differences among tectonic settings are usually related to frictional properties of faults and profiles of differential stress. However, inconsistency arises if low-angle normal and thrust faults are attempted to be explained using the friction of faults; a clear mismatch also occurs comparing results obtained in laboratory faults with geodetic and geophysical inversion in the case of tectonic faults; at last, notwithstanding the large variability of the observed friction coefficients, no correlation has been ever highlighted between friction on the fault plane and the angle of dip. In the present paper, we analyze this issue by a different viewpoint. We consider stress gradients produced by the competing action of gravitational and tectonic stress. We show that the variability of the angle of dip in different tectonic settings can be explained in light of an optimization criterion: faults tend to be oriented along the direction of the largest shear stress gradient in any tectonic setting, i.e., the stress concentrates in a smaller crustal volume. We highlight that the dip angle is affected by some mechanical properties of rocks, e.g., the Poisson's ratio, and stress concentration in the crust. We also explain the observation of active misaligned faults as due to the local weaknesses of crustal volumes. According to Mohr-Coulomb criteria, when a slip surface already exists, displacement is allowed over a range of angles (e.g., Sibson, 1985, 1991, 2000), depending on the stress tensor, the static friction and fault friction (Byerlee, 1978), fluid pressure (Sibson, 1981, 1992), cohesion or roughness in the case of relatively low stress (Goodman, 1991; Patton, 1966). Therefore, a wide variability of fault activation dip may occur. However, the misaligned faults are affected by lower stress gradients along rake than the optimally oriented slip planes in agreement with computational simulations, structural and seismological observations (Chu et al., 2021; Duan et al., 2019; Saucier et al., 1992); therefore, they have higher probability of being associated with lower seismogenic potential, or even with aseismic behavior. Our model can reproduce the observed distribution of dip angles, as proven by the statistical analysis of a wide set of large seismic events representative of major seismicity occurred all over the world during the last decades.

Data availability

Global moment tensor event databases used in the present research are available at the following links: www.globalcmt.org/CMTsearch.html (GCMT catalog) and www.earthquake.usgs.gov/earthquakes/search/ (USGS catalog).

Author Contributions

D.Z. conceived the key ideas, model, performed the analysis, contributed to its interpretation. C.D. inspired this work, realized the geological interpretation of results and led the research project. C.D. and D.Z. prepared the figures, wrote the early draft and edited the final manuscript; both authors agreed with the published version of the article.

Declaration of Competing Interest

The authors declare that they have no known competing financial interests or personal relationships that could have appeared to influence the work reported in this paper.

Acknowledgments

We thank the editor and two anonymous reviewers for their comments and suggestions. We are grateful to Giacomo Pozzi and Giulia Schirripa Spagnolo for fruitful discussions. The research is supported by the INGV.

References

Aifantis, E.C., 2020. A concise review of gradient models in mechanics and physics. Frontiers in Physics 7, 239.
Anderson, E., 1951. The dynamics of faulting and dyke formation with application to britain, 206 pp. Oliver and Boyd, White Plains, NY.
Anderson, E.M., 1905. The dynamics of faulting. Transactions of the Edinburgh Geological Society 8 (3), 387–402.
Anooshehpoor, A., Brune, J.N., 1994. Frictional heat generation and seismic radiation in a foam rubber model of earthquakes. pure and applied geophysics 142 (3), 735–747.
Axen, G.J., 1992. Pore pressure, stress increase, and fault weakening in low-angle normal faulting. Journal of Geophysical Research: Solid Earth 97 (B6), 8979–8991.
Bird, P., Kong, X., 1994. Computer simulations of california tectonics confirm very low strength of major faults. Geological Society of America Bulletin 106 (2), 159–174.
Brudy, M., Zoback, M.D., Fuchs, K., Rummel, F., Baumgärtner, J., 1997. Estimation of the complete stress tensor to 8 km depth in the KTB scientific drill holes: Implications for crustal strength. Journal of Geophysical Research: Solid Earth 102 (B8), 18453–18475.
Byerlee, J., 1978. Friction of rocks. In: Rock friction and earthquake prediction. Springer, pp. 615–626.
Cartwright-Taylor, A., Mangriotis, M.-D., Main, I.G., Butler, I.B., Fusseis, F., Ling, M., Andò, E., Curtis, A., Bell, A.F., Crippen, A., et al., 2022. Seismic events miss important kinematically governed grain scale mechanisms during shear failure of porous rock. Nature communications 13 (1), 1–14.
Chu, S.X., Tsai, V.C., Trugman, D.T., Hirth, G., 2021. Fault interactions enhance high-frequency earthquake radiation. Geophysical Research Letters 48 (20).
Collettini, C., 2011. The mechanical paradox of low-angle normal faults: Current understanding and open questions. Tectonophysics 510 (3-4), 253–268.
Collettini, C., Tesei, T., Scuderi, M.M., Carpenter, B.M., Viti, C., 2019. Beyond byerlee friction, weak faults and implications for slip behavior. Earth and Planetary Science Letters 519, 245–263.
Dal Zilio, L., van Dinther, Y., Gerya, T., Avouac, J.-P., 2019. Bimodal seismicity in the himalaya controlled by fault friction and geometry. Nature communications 10 (1), 1–11.
Dewey, J.F., 1988. Extensional collapse of orogens. Tectonics 7 (6), 1123–1139.

Doglioni, C., Barba, S., Carminati, E., Riguzzi, F., 2014. Fault on–off versus coseismic fluids reaction. Geoscience Frontiers 5 (6), 767–780.
Doglioni, C., Carminati, E., Petricca, P., Riguzzi, F., 2015. Normal fault earthquakes or graviquakes. Scientific Reports 5 (1), 1–12.
Duan, B., Liu, Z., Elliott, A.J., 2019. Multicycle dynamics of the aksay bend along the altyn tagh fault in northwest china: 2. the realistically complex fault geometry. Tectonics 38 (3), 1120–1137.
Faulkner, D.R., Mitchell, T.M., Healy, D., Heap, M.J., 2006. Slip on'weak'faults by the rotation of regional stress in the fracture damage zone. Nature 444 (7121), 922–925.
Fazlikhani, H., Back, S., Kukla, P.A., Fossen, H., 2017. Interaction between gravity–driven listric normal fault linkage and their hanging-wall rollover development: a case study from the western niger delta, nigeria. Geological Society, London, Special Publications 439 (1), 169–186.
Fossen, H., 2016. Structural geology. Cambridge university press.
Goodman, R.E., 1991. Introduction to rock mechanics. John Wiley & Sons.
Healy, D., Blenkinsop, T.G., Timms, N.E., Meredith, P.G., Mitchell, T.M., Cooke, M.L., 2015. Polymodal faulting: Time for a new angle on shear failure. Journal of Structural Geology 80, 57–71.
Hickman, S.H., 1991. Stress in the lithosphere and the strength of active faults. Rev. Geophys 29, 759–775.
Jackson, J.A., White, N.J., 1989. Normal faulting in the upper continental crust: observations from regions of active extension. Journal of Structural Geology 11 (1-2), 15–36.
Kapp, P., Taylor, M., Stockli, D., Ding, L., 2008. Development of active low-angle normal fault systems during orogenic collapse: Insight from tibet. Geology 36 (1), 7–10.
Lagioia, R., Panteghini, A., 2016. On the existence of a unique class of yield and failure criteria comprising tresca, von mises, drucker–prager, mohr–coulomb, galileo–rankine, matsuoka–nakai and lade–duncan. Proceedings of the royal society A: mathematical, physical and engineering sciences 472 (2185), 20150713.
Leech, M.L., 2001. Arrested orogenic development: eclogitization, delamination, and tectonic collapse. Earth and Planetary Science Letters 185 (1-2), 149–159.
Livaccari, R.F., 1991. Role of crustal thickening and extensional collapse in the tectonic evolution of the sevier-laramide orogeny, western united states. Geology 19 (11), 1104–1107.
Melosh, H.J., 1990. Mechanical basis for low-angle normal faulting in the basin and range province. Nature 343 (6256), 331–335.
Morley, C.K., Haranya, C., Phoosongsee, W., Pongwapee, S., Kornsawan, A., Wonganan, N., 2004. Activation of rift oblique and rift parallel pre-existing fabrics during extension and their effect on deformation style: examples from the rifts of thailand. Journal of Structural Geology 26 (10), 1803–1829.
Patton, F.D., 1966. Multiple modes of shear failure in rock. 1st ISRM Congress. OnePetro.
Ranalli, G., 1995. Rheology of the Earth. Springer Science & Business Media.
Ranalli, G., Yin, Z.-M., 1990. Critical stress difference and orientation of faults in rocks with strength anisotropies: the two-dimensional case. Journal of Structural geology 12 (8), 1067–1071.
Reches, Z., 1983. Faulting of rocks in three-dimensional strain fields II. theoretical analysis. Tectonophysics 95 (1-2), 133–156.
Reches, Z., Dieterich, J.H., 1983. Faulting of rocks in three-dimensional strain fields i. failure of rocks in polyaxial, servo-control experiments. Tectonophysics 95 (1-2), 111–132.
Saucier, F., Humphreys, E., Weldon, R., 1992. Stress near geometrically complex strike-slip faults: Application to the san andreas fault at cajon pass, southern california. Journal of Geophysical Research: Solid Earth 97 (B4), 5081–5094.
Scholz, C.H., 2019. The mechanics of earthquakes and faulting. Cambridge university press.
Schueller, S., Braathen, A., Fossen, H., Tveranger, J., 2013. Spatial distribution of deformation bands in damage zones of extensional faults in porous sandstones: Statistical analysis of field data. Journal of Structural Geology 52, 148–162.
Shebalin, P., Narteau, C., 2017. Depth dependent stress revealed by aftershocks. Nature communications 8 (1), 1–8.
Sibson, R.H., 1974. Frictional constraints on thrust, wrench and normal faults. Nature 249 (5457), 542–544.
Sibson, R.H., 1981. Fluid flow accompanying faulting: field evidence and models. Earthquake prediction: an international review 4, 593–603.
Sibson, R.H., 1985. A note on fault reactivation. Journal of Structural Geology 7 (6), 751–754.
Sibson, R.H., 1991. Loading of faults to failure. Bulletin of the Seismological Society of America 81 (6), 2493–2497.
Sibson, R.H., 1992. Implications of fault-valve behaviour for rupture nucleation and recurrence. Tectonophysics 211 (1-4), 283–293.
Sibson, R.H., 1994. Crustal stress, faulting and fluid flow. Geological Society, London, Special Publications 78 (1), 69–84.
Sibson, R.H., 2000. Fluid involvement in normal faulting. Journal of Geodynamics 29 (3-5), 469–499.
Sperl, M., 2006. Experiments on corn pressure in silo cells–translation and comment of janssen's paper from 1895. Granular Matter 8 (2), 59–65.
Tan, E., Lavier, L.L., Van Avendonk, H.J.A., Heuret, A., 2012. The role of frictional strength on plate coupling at the subduction interface. Geochemistry, Geophysics, Geosystems 13 (10).
Thompson, G.A., Parsons, T., 2017. From coseismic offsets to fault-block mountains. Proceedings of the National Academy of Sciences 114 (37), 9820–9825.
Twiss, R.J., Moores, E.M., 1992. Structural geology. Macmillan.
Wang, E., Meng, K., Su, Z., Meng, Q., Chu, J.J., Chen, Z., Wang, G., Shi, X., Liang, X., 2014. Block rotation: Tectonic response of the sichuan basin to the southeastward growth of the tibetan plateau along the xianshuihe-xiaojiang fault. Tectonics 33 (5), 686–718.
Wernicke, B., Axen, G.J., 1988. On the role of isostasy in the evolution of normal fault systems. Geology 16 (9), 848–851.
Westaway, R., 1999. The mechanical feasibility of low-angle normal faulting. Tectonophysics 308 (4), 407–443.
Yin, Z.-M., Ranalli, G., 1992. Critical stress difference, fault orientation and slip direction in anisotropic rocks under non-andersonian stress systems. Journal of Structural Geology 14 (2), 237–244.
Zaccagnino, D., Doglioni, C., 2022. Earth's gradients as the engine of plate tectonics and earthquakes. La Rivista del Nuovo Cimento 45 (12), 801–881.
Zaccagnino, D., Doglioni, C., 2022. The impact of faulting complexity and type on earthquake rupture dynamics. Communications Earth & Environment 3 (1), 1–10.
Zaccagnino, D., Telesca, L., Doglioni, C., 2022. Scaling properties of seismicity and faulting. Earth and Planetary Science Letters 584, 117511.